Mode conversion of Mie plasmons at the surface of metallic atomic clusters

A. El-Khawaldeh* and H.-J. Kull†

Institute for Theory of Statistical Physics, RWTH Aachen University, 52056 Aachen, Germany

(Received 16 September 2016; revised manuscript received 26 January 2017; published 3 April 2017)

The dynamics of the Mie plasmon is described in the framework of the self-consistent quantum Vlasov theory by a reduced single-state model. The single-state model is validated by many-electron calculations for Na clusters. In this framework, collisionless damping of the Mie plasmon can be investigated for a wide range of cluster parameters by linear perturbation theory. The characteristic scaling of the damping rate with the inverse cluster radius is demonstrated. The basic damping mechanism of the Mie plasmon can be explained by a conversion of surface modes into volume modes due to the scattering by the self-consistent potential of the electron-electron interaction at the cluster boundary.

DOI: 10.1103/PhysRevA.95.043401

I. INTRODUCTION

Atomic clusters form a bridge between atoms or molecules and bulk matter. While the electron density is typically of the same order of magnitude as in solids, quantum confinement becomes relevant as the cluster size approaches the scale of the Fermi wavelength [1].

Clusters are of special interest in the field of laser-matter interaction. The efficient coupling of high laser intensities to matter is favored on the one hand by high electron densities and on the other hand by the absence of energy transport losses in bulk matter. Both requirements are usually fulfilled for atomic clusters, which typically consist of a few tens up to a few million atoms [2].

The inner ionization of clusters in high-intensity laser fields can lead to a dense plasma state with high electron temperatures [3]. Together with the background ions, inner ionization causes large space charges that result in an expansion of the cluster. Thermal and Coulomb explosions of the cluster can lead to highly energetic particles, where kinetic energies up to 500 keV in the case of electrons [4,5] and 1 MeV for ions [6] were observed.

The decrease of the electron density during the expansion enables the excitation of the characteristic dipole oscillation, known as Mie oscillation [7]. The Mie frequency is given by $\omega_M = \omega_p/\sqrt{3}$, where $\omega_p = \sqrt{4\pi n_0 e^2/m_e}$ is the plasma frequency in Gaussian cgs units, e the elementary charge, m_e the electron mass, and n_0 the electron density. Specifically, for large Na clusters with a bulk density of $n_0 = 2.65 \times 10^{22}\ \mathrm{cm}^{-3}$, the Mie plasmon occurs at the energy $\hbar\omega_M = 3.49\,\mathrm{eV}$.

The Mie resonance can be theoretically obtained most simply by treating a small homogeneous dielectric sphere in a homogeneous time-dependent electric field [8]. This treatment goes back to the work of Lord Rayleigh on the scattering of small spherical particles [9]. The more complete Mie theory applies to scattering by dielectric spheres of arbitrary size with a full account to the electromagnetic radiation field [10].

For small clusters, one can observe a dependence of the plasmon frequency on the cluster radius. As the cluster size approaches the nanoscale, the so-called spill-out effect of the electron density becomes relevant. It describes the occurrence of a nonvanishing electron density outside the cluster and is a pure quantum effect in degenerate electron gases with temperatures below the Fermi energy. The influence of the electronic spillout on the surface plasmon frequency has been investigated theoretically using time-dependent density functional theory (DFT) [11–15] and experimentally [16–19]. In particular, the jellium approximation, in which the ionic background is treated as a homogeneously charged sphere, is a well-known approach to describe simple metal clusters. This model has proven to show good results for alkali metal clusters with closed subshells [20–23]. A common feature of experiments on the Mie resonance of alkali metal clusters is a redshift of the Mie plasmon frequency with respect to the value of $\omega_M = \omega_p/\sqrt{3}$ [24]. However, the inverse trend can be observed for noble metal clusters due to the reduced s-d screening, which leads to an exclusion of the $4d$ electrons from the surface region. In particular, it was found experimentally for Ag clusters in the gas phase that the Mie resonance is blueshifted [25].

In general, the Mie oscillation in clusters is damped. Several physical mechanisms for plasmon relaxation are known to be of basic importance. As in bulk matter, collisional damping results from electron-ion collisions. The electron-ion collision frequency is independent of the cluster size and decreases with increasing temperature [24,26]. The emission of dipole radiation leads to radiation damping, which is known to become dominant for large clusters [24,27]. Apart from these elementary collisional and radiative processes, damping of the Mie plasmon can result from the collisionless dynamics of the electrons. As in homogeneous systems, Landau damping is a basic collisionless damping mechanism. It is a kinetic effect related to the velocity distribution function and is described by the Lindhard dielectric function [28]. In inhomogeneous systems, like a finite-size atomic cluster, damping of the collective electron motion can also result from surface scattering [29–31]. The surface scattering mechanism is roughly proportional to the fraction of surface electrons leading to a characteristic $1/R$ scaling of the damping rate. Surface scattering has been discussed occasionally in the literature. However, a self-consistent treatment is quite demanding, especially for large clusters. Theoretical work on the collisionless damping of the Mie plasmon has been performed in the

*amir.el@rwth-aachen.de
†kull@ilt-extern.fraunhofer.de

random-phase approximation (RPA) [32–34]. However, the authors faced a lack of information on the electron equilibrium and the confining potential of the electrons at the cluster surface. Therefore, these approaches were basically limited to a homogeneous sphere for the electron equilibrium. The RPA approach was generalized by Zaremba and Persson [31], who considered more realistic approximations of the confining electron potential in terms of a step potential or a Lang-Kohn potential [35]. In particular, they point out that due to the sensitivity of their result to the confining model potential, a self-consistent treatment is necessary. Other work has been based on hydrodynamic approaches with *ad hoc* boundary conditions at the surface of the sphere [36].

The excitation of Mie oscillations in clusters has been treated previously by classical particle simulations. In one of these works, the relaxation of an impulsively excited dipole was calculated at temperature zero with Thomas-Fermi-Vlasov simulations [37]. Due to the absence of a significant fraction of spill-out electrons in this model, the dominant damping effect resulted from bulk collisions. In later work, classical cluster simulations have been substantially improved by microscopic particle-in-cell (MicPIC) methods [38,39]. In this framework, the importance of both bulk and surface collisions as well as that of radiation damping has been demonstrated in laser-driven clusters. In addition, plasma wave dynamics within the interior of the cluster following recollisions of electrons at the cluster surface has been observed. Finally, we mention that nonlinear laser-cluster interactions lead to additional collisionless damping effects like, e.g., harmonic generation and outer ionization of the cluster [40–42].

In this work, we will present a feasible theoretical model, the single-state Vlasov model (SSVM) that allows one to calculate collisionless damping for small and moderately large weakly excited clusters in the quantum regime of Fermi-degenerate electrons. The basic problem to be considered is the linear response of the dipole moment of a small spherical cluster if the electrons are slightly shifted out of the equilibrium state. The relaxation of the surface plasmon by surface scattering requires a proper self-consistent kinetic treatment of the electron spillout and of the surface inhomogeneity. As a major result of the present work, it is found that the well-known surface plasmon decays in the collisionless non-radiative regime into volume plasmons which are associated with plasma wave excitations inside the cluster [38,39]. It is demonstrated that plasma waves are excited even in the linear regime due to surface inhomogeneities and that they contribute significantly to the damping of the Mie plasmon. In contrast to Landau damping in a homogeneous system, the surface mode is not damped by single-particle excitations. Instead, it appears that surface scattering represents a wave-wave conversion process. Mode conversion allows for the spread of energy from the surface to the volume by collective excitations. In an intermediate stage, the energy is completely converted to volume modes. The energy of these volume modes will ultimately be transferred to single-particle excitations by Landau damping or it will be irreversibly dissipated by collisions. It is noted that the surface and volume modes only exist independently in an infinitely extended system, where the surface effect can be ignored. A necessary condition for mode conversion is the presence of spill-out electrons at the surface and of a related self-consistent scattering potential of the electron-electron interaction. The damping mechanism by mode conversion will be analyzed in detail in this work, and the damping rate as well as its scaling with the cluster radius and the number of spill-out electrons will be derived. As a result, the damping rate and the fraction of spill-out electrons in the equilibrium state can be represented by two simple and closely related $1/R$ laws.

In the present work, the electron system is described as an ideal or weakly coupled quantum plasma, describing metallic clusters with delocalized electrons in the high-density and low-temperature regime. Such systems are commonly described in the framework of the self-consistent quantum Vlasov theory for the single-particle density operator [43], where exchange and correlation effects are neglected. The quantum Vlasov theory can be derived from the general Bogoliubov-Born-Green-Kirkwood-Yvon (BBGKY) hierarchy, which determines the time evolution of reduced statistical operators [44]. More general kinetic equations can account for correlations and exchange effects [45–48]. The Vlasov theory corresponds to a quantum-mechanical multistream model that will be introduced in Sec. II. It offers a computationally efficient method to treat quantum plasmas, since the plasma can be described by a finite set of wave functions. While this reduces the numerical effort drastically, the collective behavior of the electron system is still covered. It is a crucial point of this work to analyze how far the collective dynamics is already captured in a description with only a few representative electron states. It is noted that the concept of representative electron states in the quantum Vlasov theory corresponds to the quantum-mechanical analog of the quasiparticle concept in classical particle-in-cell simulations [49].

The multistream model has been applied to a $1d$ quantum plasma, where subexponential phase relaxation [28] and nonlinear wave breaking of plasmon excitations [50] were observed. In the present work, this theory is applied to a finite-size system, an atomic cluster in the jellium approximation.

In Sec. III, the equilibrium states of the electron system are calculated. The spill-out region of the electron density is of particular importance for the description of plasmon damping. This fact motivates a more detailed analysis of the surface region of the electron equilibrium. We demonstrate that the SSVM is capable of describing the spill-out region of Na clusters to a very good approximation. For the interpretation of the SSVM results, comparison is made between the SSVM and many-electron Vlasov equilibria of Na clusters. To investigate the effect of exchange and correlation interactions on the spill-out density, further comparison is made with previous DFT results [48].

In Sec. IV, cluster excitations are treated in linear perturbation theory using a partial wave expansion of the underlying Vlasov-Poisson system. A complete set of wave functions for the radial parts of the perturbation in the corresponding self-consistent potential is obtained.

In Sec. V A, the focus is put on the surface plasmon resonance. For the analysis of the Mie plasmon, the dipole motion of the electron system is studied based on the time-propagated electron wave functions. By studying the time dependence of the dipole oscillation, one can calculate the resonance frequency and damping rate of the Mie plasmon as

a function of the cluster radius. The result of the simple SSVM is compared with many-electron calculations we performed for Na clusters up to a radius of 1.2 nm. Using Ehrenfest's theorem, the equation of motion of the center of mass is derived, including a damping term due to the electron dynamics in the region exterior to the cluster system. We finally present a detailed analysis of the damping mechanism based on the dynamics of the electron density, which allows for a more precise interpretation of surface scattering in terms of a mode conversion process.

In Sec. V B, the focus is put on the volume plasmon resonance. For the identification of volume plasmons, it turned out to be instructive to study the Fourier transform of the time-propagated density at a fixed position inside the cluster. Since each mode generates a Lorentzian profile in frequency space, this allows for a calculation of the damping constants and resonance frequencies by a fitting procedure. It is found most notably for small clusters that the resonance frequencies are redshifted with respect to the ones in the large cluster limit, where the redshift increases as a function of the mode number.

II. MULTISTREAM MODEL

In the present model, the ions are treated as a homogeneously charged sphere with radius R, volume $V_{\rm ion} = (4/3)\pi R^3$, and charge density en_0, where $n_i = n_0/Z$ is the density of ions with average charge state Z. The following units are used for a plasma with density n_0 and plasma frequency $\omega_p = \sqrt{4\pi n_0 e^2/m_e}$:

$$\boldsymbol{r} = \sqrt{\frac{m_e\omega_p}{\hbar}}\boldsymbol{r}^\star, \quad t = \omega_p t^\star, \quad n = \frac{n^\star}{n_0}, \quad E = \frac{E^\star}{\hbar\omega_p},$$
$$q = \frac{q^\star}{e}, \quad \varphi = \varphi^\star\left(\frac{\hbar}{m_e\omega_p}\right)^{\frac{3}{2}}, \tag{1}$$

where $\hbar$ is the reduced Planck constant. Here, $\boldsymbol{r}$ is the position, t time, n density, E energy, q charge, and φ the wave function in dimensionless units. Dimensional quantities are denoted by a star. In some figures we use the length scale $L = \sqrt{\hbar/(m_e\omega_p)}$. The units (1) are commonly used for a harmonic oscillator with frequency ω_p. Since ω_p is the plasma frequency, these units depend on the density n_0 and are chosen for the numerical evaluation, since n_0 and all other constants besides the cluster radius R can be eliminated from the underlying equations. It is noted that the cluster radius R_{pl} in terms of these plasma units and the radius R_{at} in atomic units are related by

$$R_{at} = C\left(\frac{r_s}{a_B}\right)^{\frac{3}{4}} R_{pl}, \quad C = \frac{1}{\sqrt[4]{3}} \approx 0.76. \tag{2}$$

Here, $r_s = [3/(4\pi n_0)]^{1/3}$ denotes the Wigner-Seitz radius and a_B the Bohr radius.

The electron system is described by a statistical ensemble of N_s single-particle states $|\varphi_k\rangle$ and corresponding wave functions $\varphi_k(\boldsymbol{r},t)$, which will be called representative electron states. The probability to find a single electron in the state k is denoted by w_k. The single-particle states $|\varphi_k\rangle$ define the single-particle statistical operator

$$\rho = \sum_{k=1}^{N_s} w_k |\varphi_k\rangle\langle\varphi_k|. \tag{3}$$

In general, the time evolution of the S-particle statistical operator ($S = 1,2,\ldots,N$) is coupled to the dynamics of the $(S+1)$-particle statistical operator via the BBGKY hierarchy [44], which can be derived from the well-known von Neumann equation for the full N-particle statistical operator by partially tracing out $N - S$ particle spaces. In the case of an uncorrelated electron system, the hierarchy decouples and the time evolution of the single-particle statistical operator is governed by the quantum Vlasov-Poisson system:

$$i\,\partial_t\rho = [H,\rho], \quad H = -\tfrac{1}{2}\Delta - \phi - \phi_{\rm ext},$$
$$\Delta\phi = {\rm Tr}(\rho\hat{n}) - n_{\rm ion}, \quad \hat{n}(\boldsymbol{r}) = \delta(\boldsymbol{r} - \hat{\boldsymbol{r}}). \tag{4}$$

Here, $\hat{n}(\boldsymbol{r})$ is the particle-density operator. The potential $\phi_{\rm ext}(\boldsymbol{r},t)$ describes the interaction with an external field. The system (4) is equivalent to the self-consistent Schrödinger-Poisson system,

$$i\,\partial_t\,\varphi_k = \big[-\tfrac{1}{2}\Delta - \phi - \phi_{\rm ext}\big]\varphi_k, \tag{5a}$$
$$\Delta\phi = \sum_{k=1}^{N_s} w_k\,|\varphi_k|^2 - n_{\rm ion}, \tag{5b}$$

where $n_{\rm ion}(r) = \theta(R - r)$. In the dimensionless representation (5), the single-particle states are normalized to the ionic volume, $\langle\varphi_k|\varphi_k\rangle = V_{\rm ion}$. The probability interpretation of the wave function associates with each wave function φ_k a probability current. In this context, the system (5) is called a multistream model. Multistream models of quantum plasmas have been used in the past by various authors [43,50–52].

A large computational simplification can be gained by a reduction of the number of representative electron states in comparison to cluster calculations with $N_s = N_e/2$, where N_e is the number of electrons and each state is occupied by two electrons with opposite spin. Specifically, in this work we consider a reduced single-state Vlasov model. Here, the number of representative states is reduced to a single wave function $N_s = 1$. It will be demonstrated that the SSVM can accurately describe the spill-out density of Na clusters and the related surface damping of the Mie plasmon. As a validation of the SSVM approach, the SSVM results will be compared with the many-electron calculations we performed for moderately large Na clusters.

The representation (5) of the Vlasov theory is closely related to the well-known Hartree theory, which can be derived from the Rayleigh-Ritz variational method assuming that the total wave function is a product state. However, both models differ by the fact that the self-energy interaction term in the Poisson equation (5b) is not included within the Hartree theory. In Sec. III, we will compare the Vlasov results for the cluster equilibria with previous results in DFT which consider the local-density approximation [53] for the exchange-correlation potential ϕ_{xc}. For the comparison with the Vlasov results, we have reproduced these DFT results by adding ϕ_{xc} to the self-consistent potential ϕ in (5b). In this case, the Vlasov

equations (5) agree with the well-known Kohn-Sham equations in DFT [54].

In the present work, the time evolution of the electron states is treated by the quantum Vlasov approach (5). In the following, we consider a microcanonical description with N_s representative states and equal population probabilities $w_k = w = 1/N_s$.

III. ELECTRON EQUILIBRIUM

Prior to the interaction with the external field $\phi_{\rm ext}$, the cluster is assumed to be in or close to the equilibrium state. Equilibria with a time-independent electron density $n^{(0)}(\boldsymbol{r})$ are characterized by a set of stationary wave functions $\varphi_k^{(0)}(\boldsymbol{r})$ satisfying the time-independent Schrödinger-Poisson system:

$$H^{(0)}\varphi_k^{(0)} = \epsilon_k\,\varphi_k^{(0)}, \quad H^{(0)} = -\frac{1}{2}\Delta - \phi^{(0)}, \tag{6a}$$

$$\Delta\phi^{(0)} = n^{(0)} - n_{\rm ion}, \quad n^{(0)} = \sum_{k=1}^{N_s} w\,\left|\varphi_k^{(0)}\right|^2. \tag{6b}$$

In the following, spherically symmetric equilibria are considered which are characterized by three quantum numbers (nlm). The equilibrium wave functions can be separated into a radial part $R_{nl}(r)$ and the spherical harmonics $Y_{lm}(\theta,\phi)$ in the form

$$\varphi_{nlm}^{(0)}(\boldsymbol{r}) = R_{nl}(r)\,Y_{lm}(\theta,\phi). \tag{7}$$

With this ansatz, the eigenvalues ϵ_{nl} are independent of the quantum number m and the degree of degeneracy of the eigenvalue ϵ_{nl} is given by $2l+1$. It will be assumed that all states with $|m| \leqslant l$ are occupied. In this case, spherical symmetry of the density in (6b) follows from the addition theorem:

$$\sum_{m=-l}^{l} |Y_{lm}|^2 = \frac{2l+1}{4\pi}. \tag{8}$$

To determine the equilibrium quantum numbers for a given number of representative states N_s, one has to assign to each electron state quantum numbers (nlm). Since there are many possible configurations for a given N_s, one has to choose the configuration which minimizes the total energy. For the calculation of the equilibrium states defined in (6), a relaxation method is chosen [55]. This method is briefly described.

Since equilibrium wave functions can be classified according to the quantum numbers n,l, and m, an ansatz

$$\varphi_{nlm}(\boldsymbol{r},t) = N_{nl}(r,t)Y_{lm}(\theta,\phi) \tag{9}$$

is chosen for the single-particle states. In this case, the system of equations (5) reduces to a set of equations for the radial wave functions N_{nl}. This system is solved in imaginary time $t = -i\tau$. The resulting equations read

$$-\partial_\tau\, N_{nl} = -\left[\frac{1}{2}\Delta_l + \phi\right]N_{nl},$$

$$\Delta_r\,\phi = \sum_{l,n} w\,\frac{2l+1}{4\pi}\,|N_{nl}|^2 - n_{\rm ion}. \tag{10}$$

TABLE I. Electron configuration of a Na cluster with $R = 10.8$ and $N_s = 99$.

l	N_l	$n=1$	$n=2$	$n=3$	$n=4$
0	4	s^2	s^2	s^2	s^2
1	3	p^6	p^6	p^6	
2	3	d^{10}	d^{10}	d^{10}	
3	2	f^{14}	f^{14}		
4	2	g^{18}	g^{18}		
5	1	h^{22}			
6	1	i^{26}			
7	1	k^{30}			

For the imaginary-time propagation, we choose initial states of the form

$$N_{nl}(r,0) \sim \exp\left(-(r-r_l)^2\right), \quad r_l = \frac{l}{l_{\rm max}}R. \tag{11}$$

Since the imaginary-time propagation neither conserves the norm of a wave function nor the angle between two electron states, it is necessary to normalize the wave functions after each time step of wave propagation in order to stick to the subspace of neutrally charged clusters. Furthermore, to ensure the orthogonality of the wave functions, a Gram-Schmidt process is applied to the wave functions N_{nl} which correspond to the same quantum number l after each time step. For large times τ, the solutions $N_{nl}(\boldsymbol{r},\tau)$ converge to the energetically lowest-lying equilibrium states defined by Eqs. (6) and (7):

$$\lim_{\tau\to\infty} N_{nl}(r,\tau) = R_{nl}(r). \tag{12}$$

As a reference example, we will consider a sodium cluster with a well-known equilibrium state [48]. The parameters of the sodium cluster are a bulk Wigner-Seitz radius of $r_s = 3.93\,a_B$ [56] and an electron number of $N_e = 198$. In the jellium model, the negative charge of the electrons is compensated by a positive charge, distributed homogeneously over a sphere of radius R. The radius of the sphere is $R = N_e^{1/3} r_s$, yielding the numerical values $R_{at} = 22.9$ in atomic units and $R_{pl} = 10.8$ in the present plasma units, which corresponds to a sodium cluster with radius 1.2 nm. The electron configuration of this equilibrium state can be found in [48] and is shown in Table I using the common spectroscopic notation of atomic physics. Due to the spin degeneracy, two electrons can be assigned to a single spatial wave function. One therefore requires $N_s = N_e/2 = 99$ electron states. These can be labeled by the orbital quantum numbers (nlm). For each quantum number l, there is a set of N_l occupied states with different n numbers $n = 1,2\ldots,N_l$ and a set of $2l+1$ occupied states with different m numbers $m = 0, \pm1, \ldots, \pm l$. All together, the number of electron states can be written as

$$N_s = \sum_{l=0}^{l_{\rm max}} (2l+1)N_l. \tag{13}$$

For the sodium cluster, the sequence of electron orbitals representing the order of filling of electron states up to $N_e = 198$ is given by

$$1s^2\ 1p^6\ 1d^{10}\ 2s^2\ 1f^{14}\ 2p^6\ 1g^{18}\ 2d^{10}\ 1h^{22}\ 3s^2\ 2f^{14}\ 1i^{26}\ 3p^6\ 1k^{30}\ 2g^{18}\ 3d^{10}\ 4s^2.$$

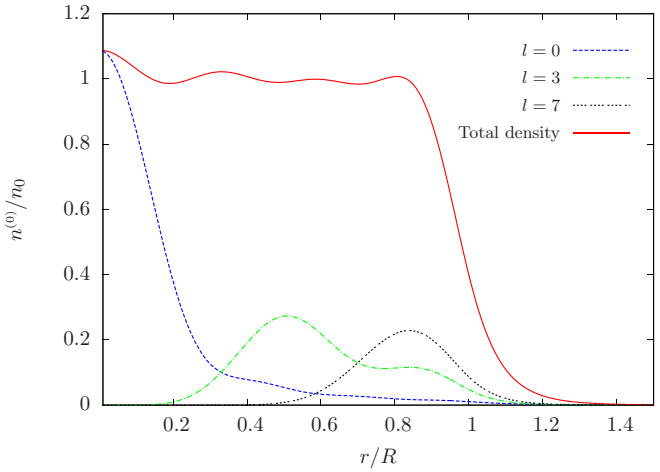

FIG. 1. Equilibrium density of a Na cluster with $R = 10.8$ and $N_s = 99$ in the Vlasov model. The figure shows the total electron density $n^{(0)}(r)$ as well as the electron densities $n_l^{(0)}(r)$ of different electron shells.

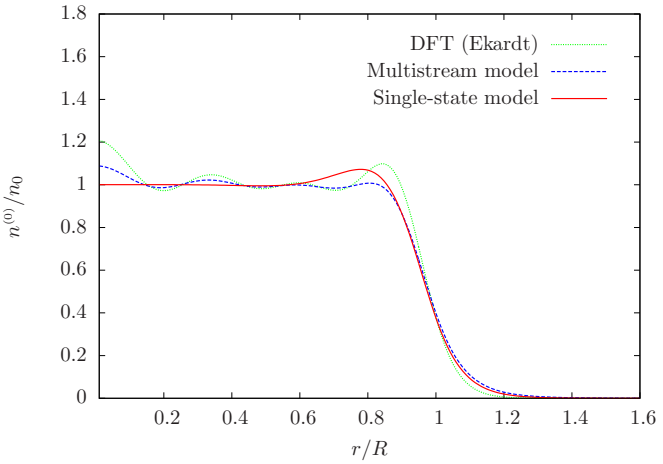

FIG. 2. Equilibrium density $n^{(0)}(r)$ of a Na cluster. The equilibrium consists of $N_e = 198$ electrons neutralized by a homogeneous ion sphere with radius $R = 10.8$ in plasma units and $R_{at} = 22.9$ in atomic units. The DFT result was first calculated by Ekardt [48] with the exchange-correlation potential introduced by Gunnarsson and Lundqvist [53]. It is compared to the present multistream Vlasov model, neglecting exchange-correlation effects, and with the reduced single-state Vlasov model. The density of the spill-out electrons can be rather accurately described by the single-state approach.

In the following, we briefly discuss the structure of the equilibrium density. Figure 1 shows the calculated equilibrium density. Besides the total electron density $n^{(0)}(r)$, the electron densities $n_l^{(0)}(r)$ of electrons with a fixed angular momentum l are plotted:

$$n_l^{(0)}(r) = \sum_{n=1}^{N_l} w \, \frac{2l+1}{4\pi} \, |R_{nl}|^2. \tag{14}$$

As shown, the cluster equilibrium exhibits a shell structure [23], where electrons with higher angular momentum are located closer to the cluster surface. The electron density decays exponentially outside the cluster. This behavior, known as the spill-out effect, is a pure quantum-mechanical effect at $T = 0$. In the case of a classical system, the spillout is a thermal effect which depends on T and which vanishes at $T = 0$. For a quantum system, the spill-out effect is essentially independent of the temperature for $T \lesssim E_F$. It leads to an effective lack of electrons on the inner side of the cluster surface. The resulting positive surface charge is screened by electrons inside the cluster, which leads to a local maximum of the electron density close to the cluster surface (see Fig. 1).

We now compare the equilibrium density of the present Vlasov calculations with previous DFT calculations and with reduced SSVM calculations. The DFT results are recalculations of the work of Ekardt [48] for the same parameters. The difference to the present Vlasov calculations is an additional exchange-correlation potential in local-density approximation, taken from Gunnarsson and Lundqvist [53]. The SSVM calculations are Vlasov calculations with only one spherically symmetric equilibrium wave function, $\varphi_{100}^{(0)}(r) = R_{10}(r)Y_{00}$, corresponding to the quantum numbers $n = 1$, $l = 0, m = 0$.

Figure 2 shows the equilibrium density $n^{(0)}(r)$ of the reference Na cluster as well as the equilibrium density in the SSVM. In addition, to investigate qualitatively how exchange and correlation effects modify the spill-out region of the electron density, the DFT result for the electron density in the local-density approximation is plotted. Indeed, one can see that the SSVM gives rise to a very good approximation of the many-electron density outside the ion sphere. Furthermore, the inclusion of exchange and correlation effects modifies the spill-out region only weakly. The close agreement of the density profiles in the spill-out region indicate that the SSVM is a good starting point for the analysis of the surface plasmon resonance.

It is noted that the quantum spill-out effect becomes dominant for small clusters, where electrons are weakly bound. This is shown in Fig. 3. The equilibrium densities of the SSVM are plotted for a large cluster with $R = 250$ and a small cluster with $R = 10$. As shown, the broadening of the electron density close to the cluster surface leads to an inhomogeneous surface potential. The local minimum of the self-consistent potential at the surface generates the binding and is a well-known feature of an electron gas at the surface of a metal [35]. For large clusters, the relative number of spill-out electrons is strongly reduced and the density approaches the classical behavior of a homogeneous sphere.

IV. PERTURBATION THEORY

In this work, the excitation of the electron equilibrium is considered in linear perturbation theory. In the following, we briefly describe the basic formalism of the perturbation theory.

Since the electron system is considered to be close to the equilibrium state, each electron stream $\varphi_k(\boldsymbol{r},t)$ can be characterized by a set of equilibrium quantum numbers $k = (nlm)$. In the perturbative description, the time-propagated single-particle states and the self-consistent potential are assumed to

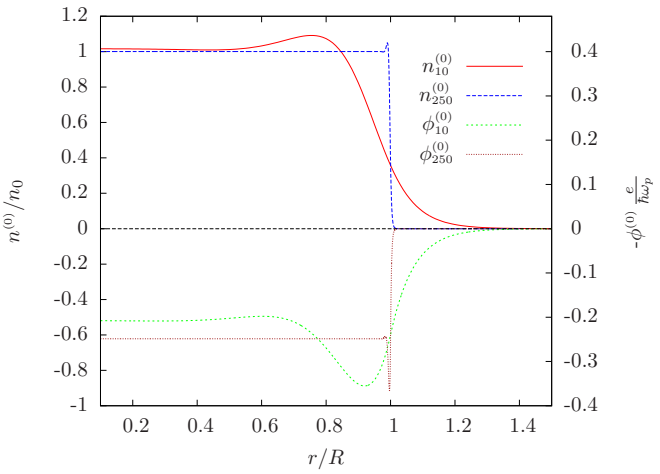

FIG. 3. Equilibrium densities $n^{(0)}(r)$ of atomic clusters (SSVM calculation). Results are shown for cluster sizes $R = 250$ and $R = 10$. In addition, the corresponding self-consistent potentials $\phi^{(0)}(r)$ in the equilibrium state are shown. It is demonstrated that the spill-out effect becomes significant for small clusters. The broadening of the electron density close to the cluster surface leads to an inhomogeneous surface potential.

be of the form

$$\begin{aligned} \varphi_{nlm}(\boldsymbol{r},t) &= \left[\varphi^{(0)}_{nlm}(\boldsymbol{r}) + \varphi^{(1)}_{nlm}(\boldsymbol{r},t)\right] e^{-i\epsilon_{nl}t}, \\ \phi(\boldsymbol{r},t) &= \phi^{(0)}(r) + \phi^{(1)}(\boldsymbol{r},t), \\ n(\boldsymbol{r},t) &= n^{(0)}(r) + n^{(1)}(\boldsymbol{r},t), \end{aligned} \tag{15}$$

where the quantities with a superscript 1 describe small perturbations of the equilibrium quantities $\varphi^{(0)}_{nlm}$, $\phi^{(0)}$, and $n^{(0)}$. The equations (5) are linearized with respect to the perturbations $\varphi^{(1)}_{nlm}$ and $\phi^{(1)}$. Then, the time evolution of the perturbed wave functions $\varphi^{(1)}_{nlm}$ is governed by the linearized Schrödinger-Poisson system:

$$i\,\partial_t\,\varphi^{(1)}_{nlm} = [H^{(0)} - \epsilon_{nl}]\varphi^{(1)}_{nlm} - [\phi_{\rm ext} + \phi^{(1)}]\varphi^{(0)}_{nlm}, \tag{16a}$$

$$\Delta\phi^{(1)} = n^{(1)} = \sum_{l=0}^{l_{\max}} \sum_{m=-l}^{l} \sum_{n=1}^{N_l} 2w\,\mathrm{Re}\left\{\varphi^{(0)*}_{nlm}\,\varphi^{(1)}_{nlm}\right\}. \tag{16b}$$

In the following, we restrict attention to azimuthally symmetric excitations of the electron system in a given sector l' of the electron density,

$$\begin{aligned} n^{(1)} &= n^{(1)}_{l'}(r,t)Y_{l'0}(\theta), \quad \phi^{(1)} = h_{l'}(r,t)Y_{l'0}(\theta), \\ \phi_{\rm ext} &= -v_{l'}(r,t)\,Y_{l'0}(\theta). \end{aligned} \tag{17}$$

This allows for an isolated study of the multipole excitations in sector l'. In particular, a perturbation with $l' = 1$ is related to the dipole oscillation of the electron system.

The perturbation theory is set up with a partial wave expansion of the perturbed wave functions $\varphi^{(1)}_{nlm}$ in terms of spherical harmonics $Y_{lm}(\theta,\varphi)$,

$$\varphi^{(1)}_{nlm}(\boldsymbol{r},t) = \sum_{\bar{l}\in M_{l'l}} g_{nl\bar{l}}\,(r,t)\,C_{l'0lm\bar{l}}\,Y_{\bar{l}m}(\theta,\phi), \tag{18}$$

where the possible quantum numbers $\bar{l}$ of this expansion are restricted to the set

$$M_{l'l} = \{|l'-l|, |l'-l|+2, |l'-l|+4, \ldots, l'+l\}. \tag{19}$$

The constants C are given in terms of the well-known Clebsch-Gordan coefficients by the relation

$$\begin{aligned} C_{l'm'lm\bar{l}} = &\sqrt{\frac{(2l'+1)(2l+1)}{4\pi(2\bar{l}+1)}} \\ &\times \langle l\ l'\,m\,m'\,|\,\bar{l}\,m\rangle\langle l\ l'\,0\,0\,|\,\bar{l}\,0\rangle. \end{aligned} \tag{20}$$

The cardinality of the set (19) is given by $|M_{l'l}| = \min(l,l') + 1$. In summary, the time evolution of a single-electron perturbation $\varphi^{(1)}_{nlm}$ is determined by $|M_{l'l}|$ radial wave functions $g_{nl\bar{l}}$ which are independent of the quantum number m. The time evolution of the radial wave functions and the radial part of the potential is governed by the following system of equations:

$$i\,\partial_t\,g_{nl\bar{l}} = H^{(0)}_{nl\bar{l}}\,g_{nl\bar{l}} + R_{nl}(v_{l'} - h_{l'}), \tag{21a}$$

$$\Delta_{l'}\,h_{l'} = \sum_{l=0}^{l_{\max}} \sum_{n=1}^{N_l} \sum_{\bar{l}\in M_{l'l}} 2w\,D_{l'\bar{l}l}\,\mathrm{Re}\{R^*_{nl}\,g_{nl\bar{l}}\}, \tag{21b}$$

where the equilibrium Hamiltonian $H^{(0)}_{nl\bar{l}}$ is given by

$$H^{(0)}_{nl\bar{l}} = -\frac{1}{2}\Delta_{\bar{l}} - \phi^{(0)} - \epsilon_{nl}, \quad \Delta_l = \Delta_r - \frac{l(l+1)}{r^2}. \tag{22}$$

Here, Δ_r is the radial part of the Laplacian. The coupling constants D are given by

$$D_{l'\bar{l}l} = \sum_{m=-l}^{l} (-1)^m\,C_{l(-m)\bar{l}m\,l'}\,C_{l'0lm\bar{l}}. \tag{23}$$

All dynamical quantities in this work will be calculated based on the time-propagated wave functions $g_{nl\bar{l}}$. For a given electron equilibrium and a perturbation in sector l' of the electron density, the linear perturbation theory requires a time propagation of in total

$$N_p = \sum_l N_l(\min(l,l')+1) \tag{24}$$

radial wave functions based on time-dependent Schrödinger equations in one dimension and a single Poisson equation for the radial part $h_{l'}$ of the self-consistent potential. The Schrödinger equations (21a) are solved with an implicit Crank-Nicolson scheme [57,58].

V. PERTURBATION RESULTS

A. Surface plasmon resonance

In this chapter, the excitation of the cluster equilibrium is investigated based on the perturbation theory presented in Sec. IV. In the first part, the main focus will be put on the surface plasmon resonance and, in particular, on the dipole sector $l' = 1$.

As a prestep of the investigation, it is analyzed which region of the electron density is responsible for the surface effects of the Mie plasmon. Here, it turned out to be instructive to derive the equation of motion for the center of mass (c.m.). This provides a deeper insight of how the c.m. motion is affected

by electrons located outside the ion sphere in the equilibrium state. With the help of Ehrenfest's theorem, the equation of motion for the c.m.,

$$\boldsymbol{R}(t) = \frac{1}{N_s}\sum_{k=1}^{N_s}\frac{\langle\varphi_k(t)|\boldsymbol{r}|\varphi_k(t)\rangle}{\langle\varphi_k(t)|\varphi_k(t)\rangle}, \tag{25}$$

reads

$$\ddot{\boldsymbol{R}} + \omega_M^2\boldsymbol{R} = \frac{1}{N_s}\sum_{k=1}^{N_s}\frac{\langle\varphi_k|\boldsymbol{F}_{sc}|\varphi_k\rangle}{\langle\varphi_k|\varphi_k\rangle}, \quad \omega_M = 1/\sqrt{3},$$

$$\boldsymbol{F}_{sc} = -\omega_M^2\boldsymbol{r}\left(\frac{R^3}{r^3} - 1\right)\theta(r-R), \tag{26}$$

where the electron-electron interaction cancels due to the action-reaction law. The motion of the c.m. corresponds to that of a harmonic oscillator with an additional force that is determined by the ensemble average of the operator $\boldsymbol{F}_{sc}$. This operator contributes only outside the ion sphere and takes into account the surface effects of the dynamics. The surface term in (26) couples to the spill-out density

$$n_{\rm out}(r,t) = n(r,t)\,\theta(r-R) \tag{27}$$

of the electron system,

$$\frac{1}{N_s}\sum_{k=1}^{N_s}\frac{\langle\varphi_k|\boldsymbol{F}_{sc}|\varphi_k\rangle}{\langle\varphi_k|\varphi_k\rangle} \sim \int_{\mathbb{R}^3} n_{\rm out}\,\boldsymbol{F}_{sc}\,d^3r$$

$$= \frac{1}{N_s}\sum_{k=1}^{N_s} 2{\rm Re}\int_{\mathbb{R}^3}\varphi_k^{(0)*}\theta(r-R)\varphi_k^{(1)}\boldsymbol{F}_{sc}d^3r, \tag{28}$$

where we have evaluated the density in linear order as defined in (16b). This relation shows explicitly that only spill-out electrons with

$$\varphi_k^{(0)}\,\theta(r-R) \neq 0 \tag{29}$$

contribute to the surface term and will thus affect the harmonic motion of the c.m. Since only electrons which are located close to the cluster surface spill out into the vacuum, the detailed electron distribution inside the cluster is not essential for the motion of the c.m.. This observation suggests that an accurate description of the plasmon dynamics requires a good description of the density spillout in the equilibrium state. It was demonstrated in Sec. III that already the SSVM with $N_s = 1$ leads to a very good description of the spill-out region. Thus, the SSVM is a good starting point for the analysis of the Mie plasmon.

The advantage of the SSVM arises from the fact that the numerical effort can be reduced drastically. This simplification is especially helpful when it comes to parameter studies, where one has to calculate a large number of cluster equilibria over a wide range of cluster sizes. According to the linear perturbation theory defined in Sec. IV, the electron dynamics within the SSVM is described by a single radial wave function $g_{10l'}(r,t)$, using $N_p = \min(0,l') + 1 = 1$.

In the following, the results for the surface plasmon resonance are presented. Thereby, results of the SSVM will be compared with many-electron calculations for Na clusters.

The classical frequency $\omega_{l'}$ of the surface plasmon resonance can be calculated analytically in the limit $R \to \infty$ using Maxwell's equations in combination with the dielectric function of a cold plasma at wave number $k = 0$. For a perturbation in the sector l' of the electron density, one obtains $\omega_{l'} = \sqrt{l'/(2l'+1)}$. In the case $l' = 1$, the frequency corresponds to the frequency ω_M of the Mie plasmon. In the following, perturbations of the dipole sector are investigated, where the perturbation is chosen such that the dynamics is azimuthally symmetric along the z axis. The time evolution of the z component of the c.m. (25) is calculated based on the time-propagated wave functions $g_{nl\bar{l}}(r,t)$ up to linear order,

$$Z(t) = \frac{1}{V_{\rm ion}}\int_{\mathbb{R}^3} n^{(1)}(\boldsymbol{r},t)\,z\,d^3r$$

$$= \frac{1}{V_{\rm ion}}\sqrt{\frac{16\pi}{3}}w\sum_{l,n}\sum_{\bar{l}\in M_{1l}} D_{1\bar{l}l}$$

$$\times \int_{\mathbb{R}} {\rm Re}\{R_{nl}^*\,g_{nl\bar{l}}\}r^3dr. \tag{30}$$

First, the results of the SSVM are presented. To generate a finite dipole moment at $t = 0$, a uniform shift of the equilibrium density along the z axis is considered. Up to linear order in the displacement δ, this yields

$$n(\boldsymbol{r},0) = n^{(0)}(\boldsymbol{r} - \delta\,\hat{\boldsymbol{e}}_z) = \left|\varphi_{100}^{(0)}\right|^2(\boldsymbol{r} - \delta\,\hat{\boldsymbol{e}}_z)$$

$$\approx n^{(0)}(r) - 2\delta\,{\rm Re}\left\{\left(\partial_z\,\varphi_{100}^{(0)}\right)\varphi_{100}^{(0)*}\right\}$$

$$= n^{(0)}(r) - 2\delta\,{\rm Re}\left\{\left(\partial_r\,\varphi_{100}^{(0)}\right)\varphi_{100}^{(0)*}\right\}\sqrt{\frac{4\pi}{3}}Y_{10}. \tag{31}$$

Comparing the initial condition for the density with the definition of the density perturbation defined in (21b), the displacement corresponds to an initial wave function $[D_{110} = 1/(4\pi)]$

$$g_{10\,1}(r,0) = -\sqrt{\frac{4\pi}{3}}\,\delta\,\partial_r\,R_{10}(r). \tag{32}$$

Figure 4 shows the time evolution of the z component of the c.m. for an initial displacement of $\delta = 0.1$. One can confirm that the motion of the c.m. corresponds to that of a damped harmonic oscillator with frequency ω and damping rate γ. This result shows that the surface term in (26) and the related density spillout give rise to an exponential damping of the Mie plasmon. The plasmon parameters γ and ω can be calculated by a fit using the model function

$$Z(t) = Z_0\cos(\omega t)e^{-\gamma t}. \tag{33}$$

This behavior is also confirmed for higher multipole excitations with $l' > 1$. Besides the damping effect, one can see that the frequency of motion ω is smaller for the small cluster with $R = 10$. As visible in Fig. 4, the damping effect is more pronounced for the smaller cluster. In this case, the spillout of the electron density in the equilibrium state is more pronounced (see Fig. 3).

The decay of the c.m. is associated with an energy loss of the collective electron motion. We briefly describe how the energy of the initial excitation is transferred to the cluster. It is a basic feature of the electrostatic Vlasov theory (5) that the

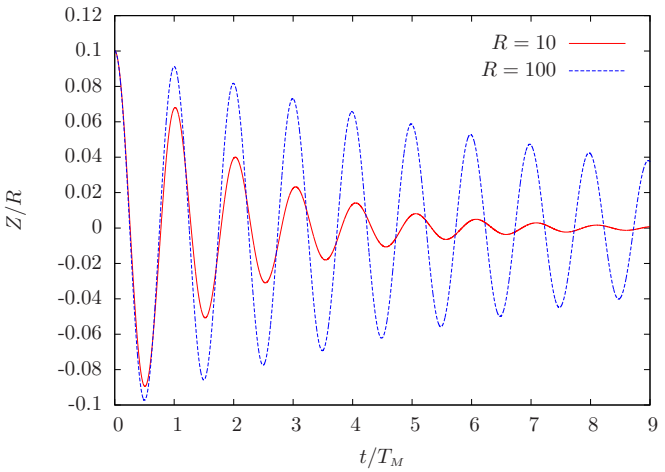

FIG. 4. Time evolution of the center of mass (SSVM calculation). The z component $Z(t)$ of the center of mass is shown for two cluster radii $R = 10$ and $R = 100$. The initial electron distribution is chosen as a shifted equilibrium distribution with displacement $\delta = 0.1$.

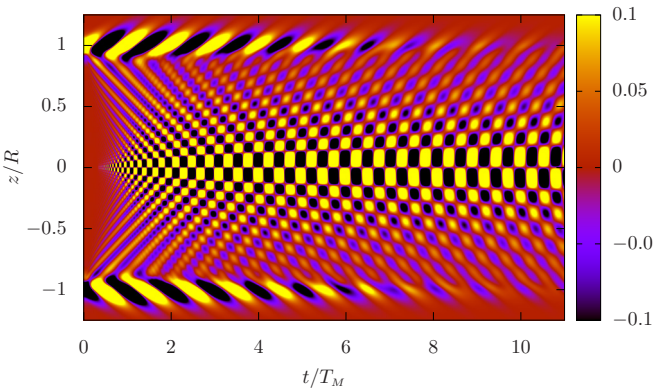

FIG. 6. Density perturbation $n^{(1)}$ of the electron system as a function of time (SSVM calculation). The density is evaluated along the z axis with $x = y = 0$. One can recognize the conversion of the surface mode into volume modes by surface scattering. The parameters are $R = 30$ for the cluster radius and $\delta = 0.5$ for the initial perturbation.

average energy

$$\langle E\rangle = \langle T\rangle + \langle V\rangle, \quad V = -\phi_{\text{ion}} - \tfrac{1}{2}\phi_{ee}$$

of the electron system is conserved if the external field is switched off, $\phi_{\text{ext}} = 0$. Here, ϕ_{ion} is the electrostatic potential of the ions and ϕ_{ee} the Hartree potential of the electron-electron interaction. The factor $1/2$ has to be taken into account in order to avoid double counting of the electron-electron interaction energy. In the following, the partition of the excitation energy into kinetic and potential energy is studied as a function of time. Figure 5 shows the evolution of the kinetic and potential energies per electron for a cluster with radius $R = 10$ and an initial displacement of $\delta = 0.1$. The corresponding motion of the c.m. is given in Fig. 4. The total energy is very well

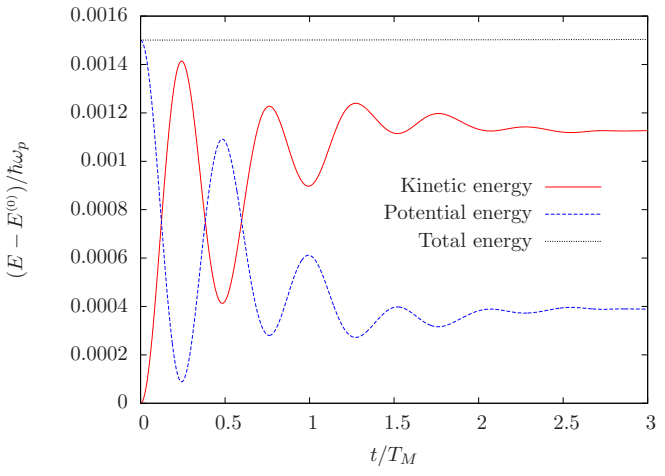

FIG. 5. Expectation values of the kinetic and potential energy per electron as a function of time (SSVM calculation). The parameters are $R = 10$ for the cluster radius and $\delta = 0.1$ for the initial perturbation. The energies are measured with respect to their corresponding equilibrium values $E^{(0)}$. It is shown that the initial excitation energy is partitioned into kinetic and potential energies, which become stationary at the end of the calculation.

conserved up to the end of the calculation. The initial potential energy becomes reduced and is largely converted into kinetic energy. It can be seen that the energies oscillate with half of the Mie period and relax together with the dipole oscillation to constant values at the end of the calculation. Since the average position and momentum vanish for large times, this result indicates that the excitation energy is contained in fluctuations of the electron system.

To gain an understanding of the residual fluctuations of cluster excitations, we studied the dynamics of the electron density. Figure 6 shows the time evolution of the density perturbation $n^{(1)}$ along the z axis with $x = y = 0$. For the calculation, we chose a cluster with radius $R = 30$. The initial electron perturbation is again produced by a rigid shift with $\delta = 0.5$. As shown in Fig. 6, the density perturbation $n^{(1)}$ is located near the cluster surface at $t = 0$, since the equilibrium density $n^{(0)}$ is almost uniform inside the cluster. The initial density overshoot at $z \approx R$ follows from the fact that the electron system is shifted in the positive z direction. From the time evolution one can see an oscillatory behavior of the density at the cluster surface on the time scale of the Mie period T_M which is related to the collective electron oscillation relative to the ion sphere. After each half period of the oscillation, particle streams are emitted from the cluster surface which move into the cluster. These streams partially result from a reflection of the electrons at the cluster surface, as is visible, e.g., at the end of the first half period when the electron system moves in the negative z direction. At time $t \approx T_M/2$, one can see that the density overshoot generated by incoming electrons at the lower cluster boundary splits into two streams. The stream which propagates in the positive z direction is associated with electrons which are reflected at the cluster surface, while the transmitted stream moves in the negative z direction and leaves the ion sphere. In total, the superposition of the waves propagating from the surface result in a formation of standing waves inside the cluster which are associated with volume plasmons. These modes are the subject of Sec. V B. In summary, we find that the surface scattering

leads to an energy transfer between the surface modes and the volume modes of the cluster.

In the following, the size dependence of the frequency and damping rate of surface plasmons is studied. Besides the dipole oscillation, quadrupole excitations ($l' = 2$) are also considered which couple to the quadrupole tensor,

$$Q_{ij}(t) = -\int_{\mathbb{R}^3} n(\boldsymbol{r},t)(3r_i r_j - r^2\delta_{ij})d^3r, \tag{34}$$

of the electron distribution.

The analysis in the single-state approximation is performed with cluster radii up to $R = 260$. Choosing a typical solid-state density $n_0 = 10^{23}\,\mathrm{cm}^{-3}$ for the ionic background, this covers the regime of clusters up to a radius of approximately 21 nm. In the first step, cluster equilibria are calculated over the range of cluster sizes considered. In the second step, the system is excited. The Mie plasmon ($l' = 1$) is excited by an external laser field in dipole approximation which is polarized along the z axis. In this case, the external potential ϕ_{ext} in (5) is given by

$$\phi_{\mathrm{ext}}(\boldsymbol{r},t) = -zE(t), \quad E(t) = E_0 \sin(\omega_L t). \tag{35}$$

Here, ω_L is the frequency of the laser. In the framework of the perturbative description, this yields $\nu_1(r,t) = \sqrt{4\pi/3}\, rE(t)$. After the laser is switched off, the decay of the c.m. is studied as a function of time. The plasmon parameters are determined by a fit to the function profile of the c.m. using the model function (33). Figure 7 shows the results for the damping rate γ and the resonance frequency ω of the Mie plasmon as a function of the cluster radius R. In addition, the results for the surface plasmon in the quadrupole sector ($l' = 2$) are plotted. Here, the dynamics of the element Q_{33} of the quadrupole tensor (34) is studied. Calculations were performed in the framework of both the SSVM and many-electron equilibria of Na clusters. The electron configurations we used for our calculations are given in Appendix A, where we considered clusters up to a radius of 1.2 nm with an electron number of $N_e = 198$. The treatment of the largest Na cluster in linear perturbation theory requires a time propagation of $N_p = 30$ radial wave functions according to (21).

One recognizes a significant redshift of the resonance frequencies for $R \lesssim 20$, while they tend to the bulk values $\omega_{l'} = \sqrt{l'/(2l'+1)}$ for large clusters. For the Mie plasmon ($\omega_M \approx 0.577\,3$) one calculates $\omega = 0.576\,8$ for the largest considered cluster with $R = 260$, while one obtains $\omega = 0.43$ for the smallest cluster with $R = 4$. In the following, we motivate the relationship between the spill-out effect and the redshift of the Mie plasmon.

Figure 8 shows the fraction f_{out} of spill-out electrons in the equilibrium state as a function of the cluster radius R. It is calculated based on the equilibrium density $n^{(0)}(r)$,

$$f_{\mathrm{out}} = \frac{N_{\mathrm{out}}}{N_e} = \frac{4\pi}{V_{\mathrm{ion}}}\int_R^\infty n^{(0)}\, r^2 dr. \tag{36}$$

For the smallest cluster with $R = 4$ approximately 25% of the electrons are located outside the ion sphere [59]. In the jellium model, the restoring force generated by the ions increases linearly with the radial distance inside the ion sphere. Outside the cluster, the restoring force decays Coulomb-like. For a decreasing cluster size, the fraction of spill-out electrons increases (Fig. 8). In conclusion, the fraction of electrons which feel a weaker restoring force than electrons inside the cluster increases as the cluster size decreases. This leads to a reduction of the resonance frequency compared with ω_M.

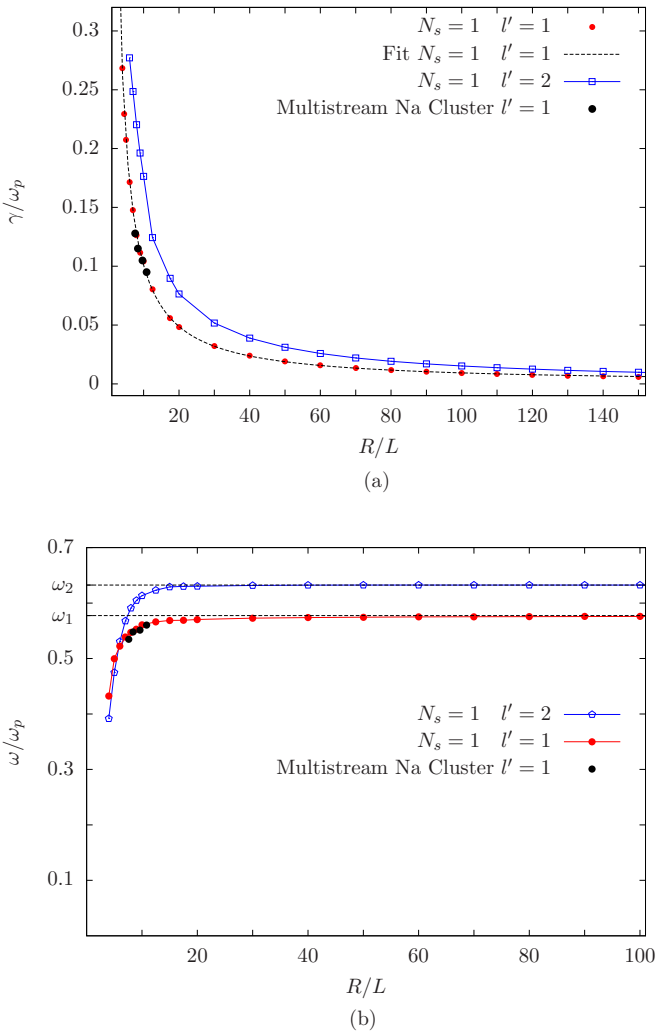

FIG. 7. Size dependence of the damping rate γ (a) and the resonance frequency ω (b) of the surface plasmon resonance in the dipole ($l' = 1$) and quadrupole ($l' = 2$) sector. The results are plotted against the cluster radius R. Calculations are performed in the single-state Vlasov model ($N_s = 1$) and with many-electron equilibria of Na clusters. The electron configurations are given in Appendix A. The data points of the single-state Vlasov model are fitted to the inverse power laws $\gamma(R) = 0.96/R^{0.99}$ for the dipole mode and $\gamma(R) = 1.54/R^{0.99}$ for the quadrupole mode.

The behavior of the damping rate γ in Fig. 7 indicates an algebraic decrease as a function of R both for the dipole and quadrupole mode. Thereby, a faster decay of the quadrupole mode can be observed. To analyze the scaling with the cluster size, a fit is performed to the data using a model function of the form

$$\gamma(R) = \frac{\alpha}{R^\beta}, \tag{37}$$

with fit parameters α and β. The fit is also shown in Fig. 7(a). As depicted, this leads to a very good description of the data

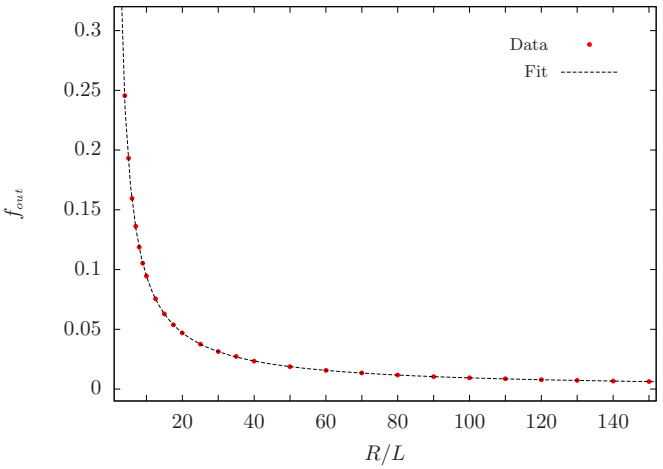

FIG. 8. Fraction of spill-out electrons in the equilibrium state as a function of the cluster radius R (SSVM calculation). The data is fitted to the inverse power law $f_{\text{out}}(R) = 0.95/R$.

in the range of cluster radii treated. The fit parameters are given in Table II. The results indicate a $1/R$ dependence of the damping rate [60] such that the damping is determined by the surface-to-volume ratio of the ion sphere. Furthermore, one can observe the significant result that the data points of the many-electron calculations fit very well to the data points of the SSVM. Although the electronic details of the Na clusters are completely neglected within the SSVM, the properties of the collective dipole oscillation are covered in a description with a single representative electron state for these reference clusters.

Transforming the power law (37) into dimensional units (1) yields ($\beta \approx 1$)

$$\gamma^\star = A\,\frac{v_{\text{p}}}{R^\star}, \quad A = \frac{\alpha}{\sqrt{2}}. \tag{38}$$

One obtains $A = 0.68$ for the dipole and $A = 1.09$ for the quadrupole mode. In our calculations we find a scaling of the the damping rate with the plasma velocity $v_p = \sqrt{2\hbar\omega_p/m_e}$. In the literature, the damping rate (38) is commonly written in terms of the Fermi velocity $v_F = (3\pi^2 n_0)^{1/3}\hbar/m_e$ [29]. Therefore we have compared both quantities, which yields a ratio of

$$\frac{v_p}{v_F} = 1.22\left(\frac{n_0}{10^{23}\text{cm}^{-3}}\right)^{-1/12}. \tag{39}$$

TABLE II. Fit parameters for the damping rate γ and the fraction f_{out} of spill-out electrons as a function of the cluster radius. A model function of the form (37) is used.

	(a) γ		(b) f_{out}	
l	α	β	α	β
1	0.96	0.99	0.95	1.00
2	1.54	0.99		

For typical electron densities n_0 within the range $10^{22}\text{cm}^{-3} < n_0 < 10^{23}\,\text{cm}^{-3}$, the ratio varies between 1.48 and 1.22. Therefore, our result differs only slightly from a scaling with the Fermi velocity over the relevant regime of electron densities. Using the definition of ω_p, the result (38) can be expressed in terms of the electron density,

$$\gamma^\star = A'\,\frac{\left(\frac{n_0}{10^{23}\text{cm}^{-3}}\right)^{\frac{1}{4}}}{\left(\frac{R^\star}{1\text{nm}}\right)}\text{fs}^{-1}, \quad A' \approx 1.44\alpha. \tag{40}$$

The result indicates that the damping rate scales with the fourth root of the electron density n_0. We calculate $A' = 1.38$ for the dipole and $A' = 2.21$ for the quadrupole mode.

It turns out (see Table II) that the fraction of spill-out electrons in the equilibrium state shows the same scaling with the inverse cluster radius. In conclusion, the damping rate of the surface plasmon scales with the fraction of spill-out electrons in the equilibrium state. In particular, for the Mie plasmon, the obtained fit parameters indicate that the dimensionless quantities $\gamma(R)$ and $f_{\text{out}}(R)$ are almost equal. In dimensional units, this yields the simple relation

$$\gamma^\star \approx \omega_p\, f_{\text{out}} \tag{41}$$

for the damping rate of the Mie plasmon.

B. Volume plasmon resonance

In the previous section, surface plasmons were treated which are related to density perturbations close to the cluster surface. The Mie plasmon can be excited by a spatially homogeneous electric field. In spatially inhomogeneous fields, produced, e.g., by external charges, other modes known as volume modes can be excited. Volume plasmons are found in each sector l' of the density perturbation. The density perturbation of volume modes is mainly located inside the cluster. In the following, the excitation is driven by an external charge distribution which is centered spherically symmetric around the point $\boldsymbol{r}' = r'\hat{\boldsymbol{e}}_z$ on the z axis. The total charge of the external distribution is given by Q. The distance between the cluster and the charge distribution is considered to be sufficiently large such that the potential of the external charges can be decomposed as ($r < r'$)

$$\phi_{\text{ext}}(\boldsymbol{r}) = \frac{Q}{|\boldsymbol{r}-\boldsymbol{r}'|} = -\sum_{l=0}^{\infty} v_l(r)\,Y_{l0}(\theta),$$
$$v_l = -\sqrt{\frac{4\pi}{2l+1}}\,\frac{Q}{r'}\left(\frac{r}{r'}\right)^l. \tag{42}$$

Volume modes turn out to couple only weakly to the multipole moments of the system such that they are not instructive for their identification. Instead, the time evolution of the perturbed wave function $g_{10l'}(r,t)$ in sector l' at the fixed radial distance $r = r_0$ inside the cluster is studied. Using this ansatz, volume modes can be identified with the Fourier transform of the

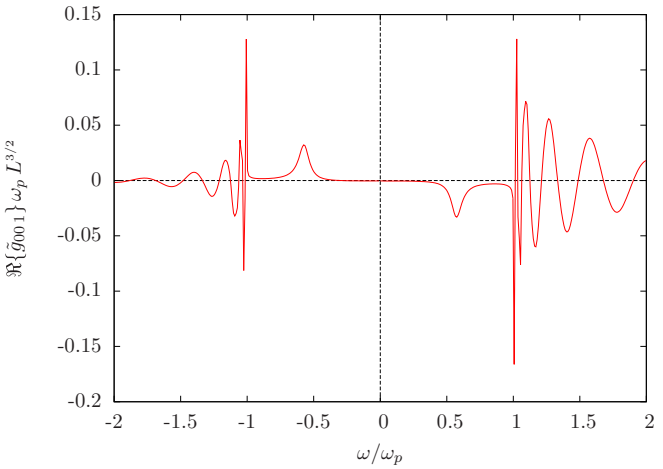

FIG. 9. Fourier transform $\mathrm{Re}\{\tilde{g}_{001}\}(r_0,\omega)$ of the time-propagated wave function in sector $l'=1$ (SSVM calculation). The wave function is analyzed at the radial distance $r_0=2$ inside a cluster of size $R=20$.

signal,

$$\tilde{g}_{00l'}(r_0,\omega)=\int_0^{T_\mathrm{f}} g_{10l'}(r_0,t)e^{i\omega t}dt, \tag{43}$$

where T_f is the final time of wave propagation. Figure 9 shows the Fourier transform of an observed wave perturbation for $l'=1$ and $R=20$. One can see a spectrally isolated peak below ω_p which is associated with the Mie plasmon. In addition, several partially overlapping peaks appear above ω_p. As shown, the width of the peaks as well as the spacing between neighboring modes increases as a function of the frequency ω. Furthermore, it is found that the mode density in frequency space increases as a function of the cluster radius.

One can conclude from the linearized equations that each fundamental mode generates a Lorentzian-shaped profile in frequency space for $T_f \gg \gamma^{-1}$. To extract the parameters (ω_n,γ_n) of volume modes, the Fourier transform (43) is fitted to a superposition of Lorentzian profiles,

$$f(\omega)=\sum_{n=1}^{N}\alpha_n\frac{\gamma_n}{(\omega-\omega_n)^2+\gamma_n^2}, \tag{44}$$

where α_n, ω_n, and γ_n are fit parameters. Due to the large number of degrees of freedom, one has to choose a good initial approximation for the fit parameters. As there is no evidence in the data to suggest the spectrum of volume modes to be limited for $\omega\to\infty$, one has to choose a cutoff N for the number of modes which are covered in this fit. The results for volume modes with $l'=1$ (see Fig. 9) are shown in Table III. Analyzing the function profile of $g_{10l'}(r,t)$ as a function of r, one finds that volume modes can be classified according to the number of nodes inside the cluster, where the density profile of the mode with mode number n has n zeros inside the cluster. The resonance frequency as well as the damping constant increase as a function of n (see Table III). For silver with $n_0=5.86\times10^{22}\,\mathrm{cm}^{-3}$, one finds a decay time of $\tau=1/\gamma=152$ fs for the volume plasmon with $n=3$ nodes.

TABLE III. Damping rates γ_n and resonance frequencies ω_n of volume plasmons in sector $l'=1$ for $R=20$. The index n characterizes the number of nodes of the corresponding density profiles.

n	1	2	3	4	5	6	7	8	9	10
ω_n	1.007	1.008	1.02	1.06	1.12	1.20	1.30	1.43	1.59	1.77
γ_n	0.0054	0.0047	0.01	0.02	0.03	0.05	0.08	0.1	0.13	0.15

We compared the lifetime of the volume plasmons with mode parameter $l'=1$ to the lifetime of the Mie plasmon. According to (37) and Table II, the damping rate of the Mie plasmon for $R=20$ is given by $\gamma\approx0.05$. From Table III one can conclude that for this cluster size the damping of the volume plasmons with mode numbers $n<6$ is weaker compared to the damping of the Mie plasmon. In particular, one recognizes that the volume plasmons with small n are long-lived compared to the Mie plasmon. This result is in agreement with the observation on the dynamics of the electron density in Fig. 6. As shown, one can clearly identify a strong signal of modes with only a few nodes n after the Mie plasmon has relaxed.

For $R\to\infty$, the frequencies of volume plasmons can be derived analytically. In sector l' of the perturbed electron density, one obtains the result (Appendix B)

$$\omega_{l'n}^2=1+\frac{1}{4}\left(\frac{z_{l'n}}{R}\right)^4,\quad n\in\mathbb{N}_0. \tag{45}$$

Here, $z_{l'n}$ are the zeros of the l'th spherical Bessel function of the first kind. The number n counts the number of nodes of the density profile. To analyze how finite-size effects modify the resonance frequencies of the volume plasmon resonance, the calculated frequencies are compared with those in the large cluster limit. Figure 10 shows the resonance frequencies for $R=20$ and $l'=1$ (Table III) together with the result (45) for $R\to\infty$. As in the case of the surface plasmon resonance, the resonance frequencies for $R=20$ are

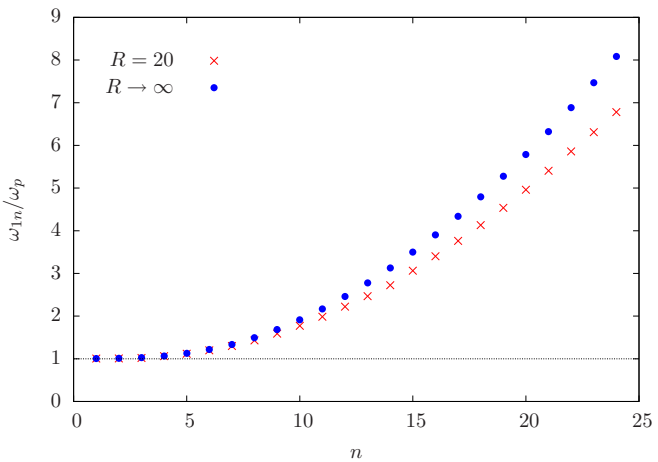

FIG. 10. Volume plasmons in sector $l'=1$ of the density (SSVM calculation). The calculated resonance frequencies ω_{1n} for $R=20$ are plotted together with the result (45) in the large cluster limit.

redshifted with respect to the ones in the large cluster limit. One recognizes that the redshift increases as a function of the mode number n.

VI. CONCLUSION

In the present work, plasmon excitations of atomic clusters were studied in the framework of the self-consistent quantum Vlasov theory. The pure quantum-mechanical spill-out effect of the electron density in the ground state was found to be crucial for the plasmon dynamics, especially for small clusters.

In a first step, the dependence of the equilibrium density on the number of representative electron states was investigated, which is an inherent parameter of the Vlasov theory. Here, the decisive electron spill-out region was found to depend only slightly on the number of representative states taken into account and on the exchange-correlation potential of DFT. In particular, it was demonstrated for a specific Na cluster that a Vlasov model in which the electron system is described by a single representative state is already sufficient to obtain the electron spillout to a very good approximation. The single-state model was then applied to obtain the dynamics of the Mie plasmon over a wide range of cluster parameters that cannot be treated with comparable numerical effort by full atomic cluster calculations.

For the Mie plasmon it was found in particular that the spillout gives rise to an exponential damping of the collective dipole motion. The resonance frequency is redshifted for small clusters with respect to its value in the large cluster limit. The damping rate shows a characteristic $1/R$ scaling. This behavior was found to be directly related to the size dependence of the fraction of spill-out electrons in the equilibrium state. A simple scaling relation (40) was obtained for the damping rate of the Mie plasmon and the quadrupole mode.

The damping mechanism of the dipole motion has been explained by mode conversion at the cluster surface. We became convinced that this mode conversion process is based on two essential preconditions. First, the electron equilibrium has to provide a significant fraction of spill-out electrons. Actually, the damping rate is found proportional to the fractional number of spill-out electrons, as demonstrated by (41). Second, the self-consistent electron-electron interaction is required to produce a coupling to the volume modes. Calculations with the ion potential only do not show damping even in the presence of electron spillout. Here, the spillout can only account for a frequency shift.

The calculations show a very good agreement of the results obtained in the SSVM with the results of many-electron calculations performed with Na clusters. Since the SSVM provides a very efficient method to describe the collective properties up to linear order, it should be instructive to investigate how far it is also applicable to nonlinear phenomena like the energy absorption in the presence of external laser fields [41,61,62].

Furthermore, a comparison to the well-known classical Mie theory [10] of light scattering by small particles provides a basic challenge. This generalization requires the solution of the complete Vlasov-Maxwell system, including magnetic interactions, and thereby it can also account for radiation damping of large clusters.

APPENDIX A: ELECTRON CONFIGURATIONS OF NA CLUSTERS

l	N_l
0	2
1	2
2	2
3	1
4	1

$R = 7.56$, $N_s = 34$

l	N_l
0	3
1	2
2	2
3	1
4	1
5	1

$R = 8.36$, $N_s = 46$

l	N_l
0	3
1	3
2	2
3	2
4	1
5	1
6	1

$R = 9.57$, $N_s = 69$

l	N_l
0	4
1	3
2	3
3	2
4	2
5	1
6	1
7	1

$R = 10.8$, $N_s = 99$

APPENDIX B: DISPERSION RELATION OF THE VOLUME PLASMON RESONANCE

The resonance frequencies of volume modes can be derived analytically for $R \to \infty$. In the case $N_s = 1$, the Schrödinger-Poisson system (5) for the wave function $\varphi(\boldsymbol{r},t)$ is equivalent to the Madelung equations

$$\partial_t n + \nabla \cdot (n\boldsymbol{v}) = 0, \tag{B1a}$$

$$\partial_t \boldsymbol{v} + (\boldsymbol{v} \cdot \nabla)\boldsymbol{v} = -\nabla U, \tag{B1b}$$

$$\Delta\phi = n - n_{\text{ion}}, \tag{B1c}$$

$$U = -\phi - \frac{1}{2}\frac{\Delta\sqrt{n}}{\sqrt{n}},$$

for the density n and the velocity field $\boldsymbol{v}$, where

$$\varphi(\boldsymbol{r},t) = A(\boldsymbol{r},t)\,\exp[iS(\boldsymbol{r},t)], \quad \boldsymbol{v} = \nabla S, \quad n = A^2. \tag{B2}$$

The equations (B1) are linearized about the equilibrium functions $n^{(0)}(\boldsymbol{r})$ and $\boldsymbol{v}^{(0)}(\boldsymbol{r})$,

$$n(\boldsymbol{r},t) = n^{(0)}(r) + n^{(1)}(\boldsymbol{r},t),$$
$$\boldsymbol{v}(\boldsymbol{r},t) = \boldsymbol{v}^{(0)}(\boldsymbol{r}) + \boldsymbol{v}^{(1)}(\boldsymbol{r},t). \tag{B3}$$

The equilibrium action S_0 is spatially constant and determined by the ground-state eigenvalue ϵ_0, $S_0(t) = -\epsilon_0 t$. Thus, $\boldsymbol{v}^{(0)} = 0$. Introducing the ansatz (B3) in (B1b), the linearized potential U reads

$$U = \underbrace{-\phi^{(0)} - \frac{1}{2}\frac{\Delta\sqrt{n^{(0)}}}{\sqrt{n^{(0)}}}}_{\epsilon_0} - \phi^{(1)} - \frac{1}{4}\Delta n^{(1)}, \tag{B4}$$

where we used that $n^{(0)} = \theta(R - r)$ for $R \to \infty$, as discussed in Sec. II. Using this result, the linearized equations for the perturbations $n^{(1)}$ and $\boldsymbol{v}^{(1)}$ read

$$\partial t\, n^{(1)} + \nabla \cdot \boldsymbol{v}^{(1)} = 0, \tag{B5a}$$

$$\partial t\, \boldsymbol{v}^{(1)} - \nabla\phi^{(1)} - \frac{1}{4}\nabla(\Delta n^{(1)}) = 0, \tag{B5b}$$

$$\Delta\phi^{(1)} = n^{(1)}. \tag{B5c}$$

Differentiating (B5a) with respect to t and acting with ∇ on (B5a), both equations can be combined using (B5c)

$$\left(1 + \partial_t^2\right) n^{(1)} + \tfrac{1}{4}\Delta^2 n^{(1)} = 0. \tag{B6}$$

This equation is solved in the frequency domain using the ansatz $\tilde{n}^{(1)}(\boldsymbol{r},\omega) = f(r,\omega)Y_{l'0}(\theta,\varphi)$ for the Fourier transform of $n^{(1)}$, taking into account azimuthally symmetric excitations. The equation for the radial part $f(r,\omega)$ reads

$$(1 - \omega^2) f + \frac{1}{4}\Delta_l^2 f = 0, \quad \Delta_l = \Delta_r - \frac{l(l+1)}{r^2}. \tag{B7}$$

Regular solutions of this equation are given by spherical Bessel functions j_l:

$$f(r,\omega) \sim j_l(kr), \quad \omega^2 = 1 + \tfrac{1}{4}k^4. \tag{B8}$$

For $R \to \infty$, the electron density vanishes outside the ion sphere. The resulting condition $j_l(kR) = 0$ leads to a quantization of the possible wave numbers k,

$$k = \frac{z_{ln}}{R}, \quad j_l(z_{ln}) = 0, \quad n = 0,1,2,\ldots, \tag{B9}$$

where n counts the number of nodes for $r < R$.

[1] B. Delley and E. F. Steigmeier, Phys. Rev. B **47**, 1397 (1993).
[2] O. F. Hagena, Z. Phys. D: At., Mol. Clust. **4**, 291 (1987).
[3] T. Ditmire, T. Donnelly, R. W. Falcone, and M. D. Perry, Phys. Rev. Lett. **75**, 3122 (1995).
[4] L. Chen, J. Park, K. Hong, I. Choi, J. Kim, J. Zhang, and C. Nam, Phys. Plasmas **9**, 3595 (2002).
[5] Y. L. Shao, T. Ditmire, J. W. G. Tisch, E. Springate, J. P. Marangos, and M. H. R. Hutchinson, Phys. Rev. Lett. **77**, 3343 (1996).
[6] E. Springate, N. Hay, J. W. G. Tisch, M. B. Mason, T. Ditmire, M. H. R. Hutchinson, and J. P. Marangos, Phys. Rev. A **61**, 063201 (2000).
[7] L. Köller, M. Schumacher, J. Köhn, S. Teuber, J. Tiggesbäumker, and K. H. Meiwes-Broer, Phys. Rev. Lett. **82**, 3783 (1999).
[8] J. Jackson, *Classical Electrodynamics*, 2nd ed. (de Gruyter, Berlin, 1975).
[9] L. Rayleigh, Philos. Mag. **12**, 81 (1881).
[10] G. Mie, Ann. Phys. (Berlin, Ger.) **330**, 377 (1908).
[11] W. Ekardt, Phys. Rev. Lett. **52**, 1925 (1984).
[12] W. Ekardt, Phys. Rev. B **31**, 6360 (1985).
[13] F. Megi, M. Belkacem, M. A. Bouchene, E. Suraud, and G. Zwicknagel, J. Phys. B: At., Mol. Opt. Phys. **36**, 273 (2003).
[14] F. Calvayrac, P. Reinhard, and E. Suraud, Ann. Phys. (NY) **255**, 125 (1997).
[15] S. Saito, G. F. Bertsch, and D. Tománek, Phys. Rev. B **43**, 6804 (1991).
[16] C. Bréchignac, P. Cahuzac, N. Kebaïli, J. Leygnier, and A. Sarfati, Phys. Rev. Lett. **68**, 3916 (1992).
[17] T. Reiners, C. Ellert, M. Schmidt, and H. Haberland, Phys. Rev. Lett. **74**, 1558 (1995).
[18] C. Bréchignac, P. Cahuzac, F. Carlier, M. de Frutos, and J. Leygnier, Chem. Phys. Lett. **189**, 28 (1992).
[19] K. Selby, M. Vollmer, J. Masui, V. Kresin, W. A. de Heer, and W. D. Knight, Z. Phys. D: At., Mol. Clust. **12**, 477 (1989).
[20] W. A. de Heer, Rev. Mod. Phys. **65**, 611 (1993).
[21] M. Brack, Rev. Mod. Phys. **65**, 677 (1993).
[22] W. Knight, W. A. D. Heer, W. A. Saunders, K. Clemenger, M. Chou, and M. L. Cohen, Chem. Phys. Lett. **134**, 1 (1987).
[23] W. D. Knight, K. Clemenger, W. A. de Heer, W. A. Saunders, M. Y. Chou, and M. L. Cohen, Phys. Rev. Lett. **52**, 2141 (1984).
[24] U. Kreibig and M. Vollmer, *Optical Properties of Metal Clusters*, Vol. 25 (Springer Science & Business Media, New York, 2013).
[25] J. Tiggesbäumker, L. Köller, K.-H. Meiwes-Broer, and A. Liebsch, Phys. Rev. A **48**, R1749 (1993).
[26] L. Spitzer and R. Härm, Phys. Rev. **89**, 977 (1953).
[27] C. Snnichsen, T. Franzl, T. Wilk, G. von Plessen, and J. Feldmann, New J. Phys. **4**, 93 (2002).
[28] W. Steffen and H.-J. Kull, Phys. Rev. E **93**, 033207 (2016).
[29] U. Kreibig and L. Genzel, Surf. Sci. **156**, 678 (1985).
[30] U. Kreibig, J. Phys. F: Met. Phys. **4**, 999 (1974).
[31] E. Zaremba and B. N. J. Persson, Phys. Rev. B **35**, 596 (1987).
[32] A. Kawabata and R. Kubo, J. Phys. Soc. Jpn. **21**, 1765 (1966).
[33] A. A. Lushnikov and A. J. Simonov, Eur. Phys. J. A **270**, 17 (1974).
[34] D. T. Thoai and W. Ekardt, Solid State Commun. **41**, 687 (1982).
[35] N. D. Lang and W. Kohn, Phys. Rev. B **1**, 4555 (1970).
[36] Y. Barash and V. Ginzburg, in *The Dielectric Function of Condensed Systems*, edited by D. K. L.V. Keldysh and A. Maradudin, Modern Problems in Condensed Matter Sciences Vol. 24 (Elsevier, New York, 1989), pp. 389–457.
[37] T. Fennel, G. F. Bertsch, and K.-H. Meiwes-Broer, Eur. Phys. J. D **29**, 367 (2004).
[38] C. Peltz, C. Varin, T. Brabec, and T. Fennel, New J. Phys. **14**, 065011 (2012).

[39] C. Varin, C. Peltz, T. Brabec, and T. Fennel, Phys. Rev. Lett. **108**, 175007 (2012).
[40] T. Fennel, K.-H. Meiwes-Broer, J. Tiggesbäumker, P.-G. Reinhard, P. M. Dinh, and E. Suraud, Rev. Mod. Phys. **82**, 1793 (2010).
[41] F. Greschik, L. Arndt, and H.-J. Kull, Europhys. Lett. **72**, 376 (2005).
[42] P. Mulser, M. Kanapathipillai, and D. H. H. Hoffmann, Phys. Rev. Lett. **95**, 103401 (2005).
[43] F. Haas, G. Manfredi, and M. Feix, Phys. Rev. E **62**, 2763 (2000).
[44] N. N. Bogolyubov and K. P. Gurov, Zh. Eksp. Teor. Fiz. **17**, 614 (1947).
[45] E. A. Uehling and G. E. Uhlenbeck, Phys. Rev. **43**, 552 (1933).
[46] D. B. Boercker and J. W. Dufty, Ann. Phys. (NY) **119**, 43 (1979).
[47] D. Kremp, T. Bornath, M. Bonitz, and M. Schlanges, Phys. Rev. E **60**, 4725 (1999).
[48] W. Ekardt, Phys. Rev. B **29**, 1558 (1984).
[49] J. M. Dawson, Rev. Mod. Phys. **55**, 403 (1983).
[50] A. Schmidt-Bleker, W. Gassen, and H.-J. Kull, Europhys. Lett. **95**, 55003 (2011).
[51] M. V. Kuzelev and A. A. Rukhadze, Phys. Usp. **42**, 603 (1999).
[52] S. V. Vladimirov and Y. O. Tyshetskiy, Phys. Usp. **54**, 1243 (2011).
[53] O. Gunnarsson and B. I. Lundqvist, Phys. Rev. B **13**, 4274 (1976).
[54] E. Runge and E. K. U. Gross, Phys. Rev. Lett. **52**, 997 (1984).
[55] A. Goldberg and J. L. Schwartz, J. Comput. Phys. **1**, 448 (1967).
[56] N. W. Ashcroft and N. D. Mermin, in *Solid State Physics* (Harcourt Brace College Publishers, San Diego, CA, 1976), p. 5.
[57] J. Crank and P. Nicolson, Math. Proc. Cambridge Philos. Soc. **43**, 50 (1947).
[58] A. Goldberg and J. L. Schwartz, J. Comput. Phys. **1**, 433 (1967).
[59] L. F. Cótica, I. A. Santos, E. M. Girotto, E. V. Ferri, and A. A. Coelho, J. Appl. Phys. **108**, 064325 (2010).
[60] J. Lermé, H. Baida, C. Bonnet, M. Broyer, E. Cottancin, A. Crut, P. Maioli, N. Del Fatti, F. Vallée, and M. Pellarin, J. Phys. Chem. Lett. **1**, 2922 (2010).
[61] F. Calvayrac, P.-G. Reinhard, E. Suraud, and C. Ullrich, Phys. Rep. **337**, 493 (2000).
[62] D. Bauer, J. Phys. B: At., Mol. Opt. Phys. **37**, 3085 (2004).